PNAS RESEARCH ARTICLE | NEUROSCIENCE

Self-renewing macrophages in dorsal root ganglia contribute to promote nerve regeneration

Rui Feng[a], Vishnu Muraleedharan Saraswathy[b,c], Mayssa H. Mokalled[b,c,d], and Valeria Cavalli[a,c,d,1]

Edited by Allan Basbaum, University of California San Francisco, San Francisco, CA; received September 16, 2022; accepted January 7, 2023

Sensory neurons located in dorsal root ganglia (DRG) convey sensory information from peripheral tissue to the brain. After peripheral nerve injury, sensory neurons switch to a regenerative state to enable axon regeneration and functional recovery. This process is not cell autonomous and requires glial and immune cells. Macrophages in the DRG (DRGMacs) accumulate in response to nerve injury, but their origin and function remain unclear. Here, we mapped the fate and response of DRGMacs to nerve injury using macrophage depletion, fate-mapping, and single-cell transcriptomics. We identified three subtypes of DRGMacs after nerve injury in addition to a small population of circulating bone-marrow–derived precursors. Self-renewing macrophages, which proliferate from local resident macrophages, represent the largest population of DRGMacs. The other two subtypes include microglia-like cells and macrophage-like satellite glial cells (SGCs) (Imoonglia). We show that self-renewing DRGMacs contribute to promote axon regeneration. Using single-cell transcriptomics data and CellChat to simulate intercellular communication, we reveal that macrophages express the neuroprotective and glioprotective ligand prosaposin and communicate with SGCs via the prosaposin receptor GPR37L1. These data highlight that DRGMacs have the capacity to self-renew, similarly to microglia in the Central nervous system (CNS) and contribute to promote axon regeneration. These data also reveal the heterogeneity of DRGMacs and their potential neuro- and glioprotective roles, which may inform future therapeutic approaches to treat nerve injury.

dorsal root ganglion (DRG) | macrophages | satellite glial cells (SGCs) | axon regeneration | peripheral nerve injury

Significance

Peripheral sensory neurons situated in dorsal root ganglia (DRG) switch to a regenerative state after nerve injury to enable nerve repair. Axon regeneration is not cell autonomous and is highly influenced by nonneuronal cells. Immune cells such as macrophages are believed to contribute to both nerve repair and neuropathic pain. Macrophages in injured peripheral nerves are well studied, but the origin and function of macrophages in the DRG (DRGMacs) remain unclear. We report the existence of four different populations of DRGMacs after nerve injury, with the largest having the capacity to self-renew and contributing to promote axon regeneration. The heterogeneity of DRGMacs may pave the way to better understand the immune mechanisms governing pain and nerve repair.

Primary sensory neurons with cell soma in dorsal root ganglia (DRG) convey sensory information from peripheral tissue to the brain. These neurons have a unique pseudounipolar morphology with a single axon, which bifurcates within the ganglion. One axon proceeds along peripheral nerves, and the other proceeds centrally along the dorsal root into the spinal cord. Lesion of the peripheral axon is followed by successful axon regeneration, whereas outgrowth of the centrally projecting axons is weak and does not lead to functional recovery, providing an opportunity to identify the mechanisms that promote axon regeneration.

Multiple studies have utilized this differential response to gain insight into the mechanisms that control the axon regeneration program, revealing that transcriptional and epigenetics events are associated with successful regeneration (1–6). Recent time course studies at the single-cell level revealed that sensory neurons respond to nerve injury by eliciting a transcriptional response that suppresses their cell identity and promotes neuronal regeneration (7). However, regulation of sensory neuron regeneration is not cell autonomous. Peripheral sensory neurons benefit from a supportive environment. Nerve injury initiates transcriptional changes in satellite glial cells (SGCs) surrounding the cell soma (8, 9) and Schwann cells surrounding the axon (10), resulting in a new transcriptional state in each cell type that promotes nerve regeneration. In addition, macrophages in the nerve, which mainly derive from circulating bone-marrow–derived precursors after injury (11–14), contribute to axon regeneration by clearing debris (11), polarizing the vascularization of the lesion (15), and regulating Schwann cell function (16).

Macrophages in the DRG (DRGMacs) also contribute to the regenerative capabilities of sensory neurons (17–21). In addition, DRGMacs contribute to the initiation and persistence of neuropathic pain after nerve injury (22) and chemotherapy-induced neuropathy (23–25). However, unlike macrophages in the nerve, circulating bone-marrow–derived precursors represent only a very small proportion of DRGMacs after nerve injury (26). The traditional view that tissue-resident macrophages derive from the bone marrow through circulating monocyte intermediates has dramatically shifted with the observation that macrophages can self-renew by local proliferation (27). However, the source and function of macrophage accumulation in the DRG after peripheral nerve injury remains unclear and whether DRGMacs have the capacity to self-renew has not been clearly established.

Author contributions: R.F., V.M.S., M.H.M., and V.C. designed research; R.F. performed research; R.F. and V.M.S. analyzed data; and R.F. and V.C. wrote the paper.

The authors declare no competing interest.

This article is a PNAS Direct Submission.

[1]To whom correspondence may be addressed. Email: cavalli@wustl.edu.

This article contains supporting information online at https://www.pnas.org/lookup/suppl/doi:10.1073/pnas.2215906120/-/DCSupplemental.

Published February 10, 2023.

To address this gap in knowledge, we first determined the source of DRGMacs after nerve injury. We established a depletion and repopulation model of DRGMacs using PLX73086, a selective inhibitor of colony-stimulating factor 1 receptor (CSF1R), which does not deplete CNS microglia because of its low blood–brain barrier (BBB) penetration (28). We then used lineage tracing to map the source of DRGMacs in response to nerve injury. We observed three sources of DRGMacs after nerve injury, in addition to the small population of circulating bone-marrow–derived precursors previously described (26). The largest population of DRGMacs derived from self-renewal by local proliferation of residual macrophages, promotes axon regeneration in vivo and contributes to the conditioning injury effect. Microglia-like cells and macrophage-like SGCs (Imoonglia) represented two other small populations. Using single-cell transcriptomics data and CellChat to simulate intercellular communication, we reveal that macrophages express the neuroprotective and glioprotective ligand prosaposin and communicate with SGCs via the prosaposin receptor GPR37L1. These data highlight that DRGMacs have the capacity to self-renew, similarly to microglia in the CNS, and contribute to promote nerve repair. These data also reveal the heterogeneity of DRGMacs and a potential neuro- and glioprotective role of macrophage-SGC communication, which may inform future therapeutic approaches to treat nerve injury.

Results

DRG Macrophages Are Depleted by Systemic PLX73086 Administration. The number of DRGMacs increases after nerve injury but circulating bone-marrow–derived precursors only account for a very small proportion of all macrophages (26). We and others previously showed that after nerve injury, the number of DRGMacs doubles and they are enriched with genes related to cell cycle (9, 22, 29). While these studies suggest that macrophage expansion originates from DRGMac proliferation, whether resident DRGMacs have the capacity to locally proliferate after nerve injury has not been clearly demonstrated. To answer this question, we sought to establish a model of DRGMac depletion and repopulation 3 d after sciatic nerve injury.

Colony-stimulating factor 1 (CSF1) binding to its receptor CSF1R regulates the survival of cells in the monocyte/macrophage lineage (30). Blocking CSF1R has been shown to deplete microglia and macrophages (28). We compared the CSF1R inhibitor PLX73086, which has low blood–brain barrier penetration, to PLX5622 (28) for their efficiency to deplete peripheral macrophages without affecting microglia in the central nervous system. Six-week-old wild-type mice were fed with PLX73086 or PLX5622-formulated diet for 21 d or control diet (referred hereafter to as CD). We quantified the number of macrophages using the Ionized calcium-binding adaptor molecule 1 (IBA1), a microglia/macrophage-specific calcium-binding protein. Less than 10% IBA1-labeled macrophages remained in the DRG and sciatic nerve after 21 d of PLX73086 or PLX5622 treatment (Fig. 1 *A*–*C* and *SI Appendix*, Fig. S1 *B*–*E*). However, unlike PLX5622, PLX73086 treatment did not affect IBA1-labeled macrophages/microglia in the lumbar spinal cord, consistent with its low blood–brain barrier permeability (*SI Appendix*, Fig. S1 *F* and *G*). These results indicate that PLX73086 has similar specificity for CSF1R as PLX5622 and can be used to target macrophage in DRG and sciatic nerve without affecting microglia in the CNS. We thus selected PLX73086 (hereafter referred to as PLX) for our studies.

We next performed a time course analysis (Fig. 1*A*). We observed that the number of IBA1-labeled DRGMacs decreased starting 1 d after PLX treatment and reached a plateau at day 14 (Fig. 1 *B* and *C*). During the 21 d of treatment, we did not observe body weight differences between the CD and PLX groups, suggesting that the treatment was well tolerated (*SI Appendix*, Fig. S1*A*). We next examined if PLX treatment causes stress in neurons by staining for activating transcription factor 3 (ATF3), an established neuronal injury marker (7, 31, 32). The percentage of neurons expressing ATF3 increased after nerve injury as expected, but ATF3 levels 14 d after PLX treatment were similar to uninjured CD control (*SI Appendix*, Fig. S1 *H* and *I*), suggesting that PLX does not cause neuronal stress. *Atf3* levels measured by qPCR further indicated that PLX treatment did not affect injury responses in DRG (*SI Appendix*, Fig. S2*D*). We then determined if DRGMacs could repopulate the DRG 3 d after removing PLX treatment. We found that the number of DRGMacs increased 3 d after switching from PLX to CD and reached levels similar to control mice (*SI Appendix*, Fig. S1 *J*–*M*). Together, these results indicate that PLX treatment depletes most macrophages, with only 10% of resident DRGMacs remaining after 14 d, allowing us to trace the repopulating macrophages after nerve injury.

Repopulated DRG Macrophages after Injury Derive in Part From Proliferation of Residual Macrophage. To trace repopulating DRG macrophages after nerve injury, we used the well-characterized *Cx3cr1*^{CreER}::Ai14 mouse model, in which tamoxifen treatment leads to tdTomato expression in macrophages and microglia (33), but not monocytes (34). *Cx3cr1*^{CreER}::Ai14 mice were treated with tamoxifen for 5 d, and then treated with either PLX or CD for 14 d (Fig. 1*D*). Immediately after sciatic nerve crush injury (SNC), PLX treatment was removed to study repopulating DRGMacs (PLX+CD) (Fig. 1*D*). Control mice received CD before and after SNC (CD+CD). Three days after SNC, the number of macrophages (labeled by IBA1) or traced macrophages (labeled by tdTomato) were similar in both PLX-treated and control groups, indicating that macrophages repopulated the DRG after injury and removal of the PLX diet (Fig. 1 *E*–*G*). More than 95% of DRG macrophages were colabeled with IBA1 and another macrophage marker, CD68, in both treatments (*SI Appendix*, Fig. S2 *A*–*C*). qPCR analysis indicated that *Aif1* levels increased similarly in control mice (CD+CD) and in mice treated with PLX+CD, further indicating that macrophages repopulate to levels similar to CD group after nerve injury (*SI Appendix*, Fig. S2*D*). We found that over 90% of the IBA1-labeled macrophages expressed tdTomato in the repopulated DRGMacs group (PLX+CD) and the control group (CD+CD) (Fig. 1 *E* and *H*), suggesting that less than 10% of the IBA1-labeled macrophages represent the small population of circulating bone-marrow–derived precursors that were identified using parabiosis (26).

We next tested if the repopulated DRGMacs after nerve injury result from proliferation of residual macrophages by injecting Bromodeoxyuridine (BrdU) once for three consecutive days, starting immediately after SNC (Fig. 1*D*). We found that ~70% of tdTomato$^+$IBA1$^+$ cells were labeled with BrdU in the repopulated DRGMac group (PLX+CD) (Fig. 1 *E* and *I*), whereas this number was lower (~40%) in the CD+CD group (Fig. 1 *E* and *I*). Less than 0.5% of IBA1-labeled macrophages that were not expressing tdTomato were labeled by BrdU after injury (Fig. 1 *E* and *J*), indicating that DRGMac proliferation is largely independent of circulating bone-marrow–derived precursors. Similar results were observed in female and male mice (*SI Appendix*, Fig. S2 *E* and *F*), suggesting that the self-renewal properties of DRGmacs after nerve injury is not gender dependent. These results suggest that macrophage depletion prior to nerve injury stimulates macrophage proliferation after injury to repopulate the DRG and indicate that DRGMac accumulation after nerve injury depends on the self-renewal properties of resident macrophages.

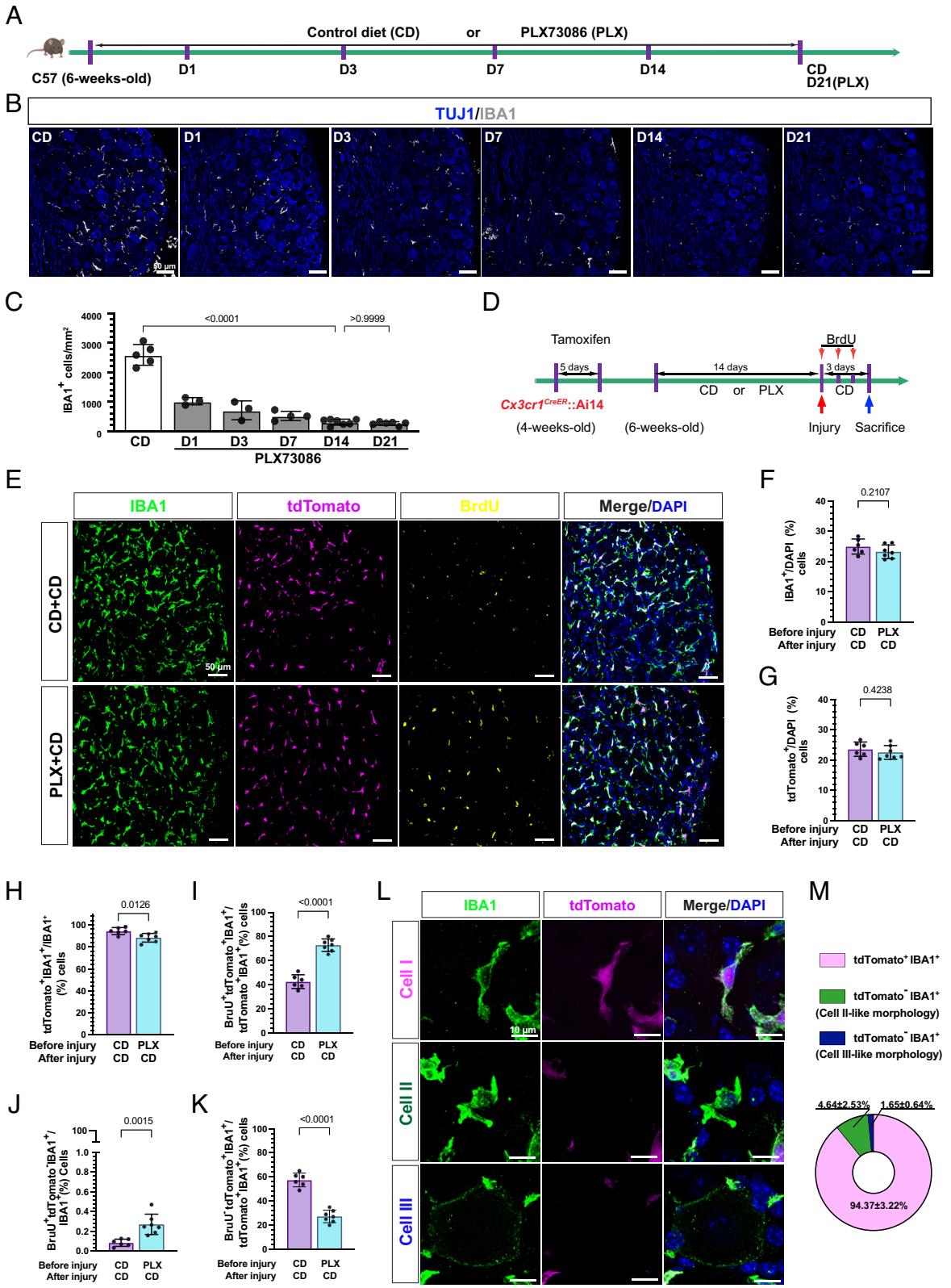

Fig. 1. A large population of DRG macrophage after injury derive from proliferation of resident macrophages. (*A*) Scheme of DRG macrophage depletion protocol and time points for examination. (*B*) Representative images showing macrophage numbers in the DRG at the indicated time after PLX administration. IBA1(red), TUJ1(blue). (Scale bars, 50 μm.) (*C*) Quantification of macrophage density (IBA1$^+$ cells/mm^2) in DRG in CD treatment and at the indicated time after PLX treatment. N = 5(CD), 3(D1), 3(D3), 4(D7), 7(D14) and 6(D21). (*D*) Scheme of genetically inducible fate mapping for DRG macrophages using the *Cx3cr1*^{CreER}::Ai14 mouse and nerve injury model. (*E*) Representative immunostaining images showing BrdU (yellow), tdTomato (magenta), IBA1 (green) and DAPI (blue) of L4 ipsilateral DRGs from the indicated treatment groups 3 d after SNC. (Scale bars, 50 μm.) (*F–K*) Quantification of the percentage of the indicated cells 3 d after nerve injury in the DRGs of mice treated with CD or PLX as indicated. IBA1$^+$ to DAPI$^+$ cells (*F*), tdTomato$^+$ cells to DAPI$^+$ cells (*G*), IBA1$^+$tdTomato$^+$ cells to IBA1$^+$cells (*H*), BrdU-labeled IBA1$^+$tdTomato$^+$ cells in IBA1$^+$tdTomato$^+$ cells (*I*), BrdU-labeled IBA1$^+$tdTomato$^-$ cells in IBA1$^+$ cells (*J*) BrdU-unlabeled IBA1$^+$tdTomato$^+$ cells in IBA1$^+$tdTomato$^+$ cells (*K*). N = 6 (CD+CD) and 7 (PLX+CD), respectively. (*L*) Representative immunostaining images of DRG 3 d after SNC showing IBA1 (green), tdTomato (magenta), and DAPI (blue). (Scale bars, 10 μm.) (*M*) Quantification of the percentage of the indicated cells in the DRG 3 d after nerve injury. N = 6. The data are presented as mean ± SD. N presented as mouse number.

To get further insights into the source of DRGMacs that do not result from self-renewal, we examined the DRGMac morphology after nerve injury (Fig.1 *L* and *M*). We observed that tdTomato-IBA1–positive cells displayed a morphology that is typical of DRGMacs (9, 22, 26) (Fig. 1 *L*, *Top*). IBA1-positive cells that were tdTomato negative displayed either a typical macrophage morphology (Fig. 1 *L*, *Middle*), or a ring-like morphology (Fig. 1 *L*, *Bottom*). The ring-like morphology is reminiscent of the Imoonglia we previously characterized (9) and consistent with other studies highlighting that SGCs are enriched in genes related to the immune system (35, 36). These results suggest that in addition to self-renewing macrophages and the small proportion of bone-marrow–derived precursors, DRGMacs include populations of different origin after nerve injury.

Microglia-Like Cells and Imoonglia Populate the DRG after Nerve Injury. A subset of macrophages in mouse peripheral nerves share features of activated microglia (12) and microglia have been reported to exit the CNS in a spinal root avulsion model in zebrafish (37). We thus hypothesized that the tdTomato cells that do not proliferate after nerve injury in the DRG may represent microglia-like cells. To test this hypothesis, we used the *Tmem119*$^{GFP/+}$ mice, which drives GFP expression under the *Tmem119* promoter. This mouse line specifically labels microglia, but does not label meningeal, perivascular, and choroid plexus macrophages in homeostatic state (38). As expected, GFP-labeled cells were not detected in the DRG of naive mice (Fig. 2*A*). However, a small number of GFP-labeled cells that were also IBA1-positive was observed on the ipsilateral side of DRGs after nerve injury (Fig. 2 *A*–*D*). These cells may represent resident DRG macrophages expressing *Tmem119* in response to injury, or microglia-like cells. To differentiate between these two possibilities, we used a method to trace microglia specifically in the CNS but not in the PNS. Microglia are known to derive from a pure early embryonic origin (39). Early embryonic precursors that give rise to yolk-sac–derived macrophages seed the brain at around embryonic day 9.5 (E9.5) (40–42), and subsequent waves of precursors, including embryonic fetal liver monocytes and hematopoietic stem cell-derived monocytes, do not engraft in the microglia pool. Therefore, to label early embryonic yolk-sac–derived macrophages, we treated *Cx3cr1*^{CreER}::Ai14 pregnant mice at E9.5 with tamoxifen (E9.5 TAM) (13, 33). Six-week-old mice were then treated with PLX for 14 d before nerve injury (Fig. 2*E*). Immediately after SNC, PLX treatment was removed, and BrdU was injected to label proliferating cells (Fig. 2*E*). tdTomato-positive cells were present in the spinal cord (*SI Appendix*, Fig. S3 *A* and *B*), indicating that the E9.5 TAM tracing method for CNS microglia was effective. Consistent with our results in adult TAM treatment, PLX administration reduced IBA1-positive cells to less than 10% in E9.5 TAM-treated mice before injury (Fig. 2 *F* and *G*) and nerve injury increased the number of IBA1-positive cells in the DRG (Fig. 2 *F* and *G*). tdTomato–positive cells in the DRG were only detected in the DRG after, but not prior, to nerve injury (Fig. 2 *F* and *H*). These cells were also labeled by IBA1, but not with BrdU (Fig. 2 *F* and *I*), suggesting that they originate from the spinal cord and do not proliferate. Together these results suggest that tdTomato-positive cells labeled by E9.5 TAM may represent microglia-like cells populating the DRG after nerve injury.

Our recent study uncovered a cell type in adult DRG, which displays the spatial arrangement of SGCs surrounding sensory neurons and express both macrophage and glial genes and increase in number after nerve injury (9). We called these cells Imoonglia. To test if a portion of the repopulated macrophages represents Imoonglia, we crossed the *Blbp*^{CreER} mice (43) (hereafter referred to as *Fabp7*^{CreER}) with Ai14 mice (Fig. 2*J*) (9). Proliferating cells were labeled by injection of BrdU once daily for 3 d, starting immediately after SNC (Fig. 2*J*). We first examined whether PLX administration affected the SGC population (*SI Appendix*, Fig. S3*C*). tdTomato-positive cells were labeled with anti-FABP7 antibodies, as expected (*SI Appendix*, Fig. S3 *D* and *E*) and PLX treatment depleted IBA1-labeled macrophages but did not affect the number of SGCs (*SI Appendix*, Fig. S3 *D*–*F*). We observed a small proportion of tdTomato-positive cells that were colabeled with IBA1, but not BrdU after nerve injury (Fig. 2 *K* and *M*), indicating that a small proportion of SGC express IBA1 after injury and do not proliferate, consistent with our previous identification of Imoonglia (9) and other studies reporting that SGCs express immune markers (44–48). Together, these results indicate that in addition to a very small number of circulating bone-marrow–derived precursors (26), three other DRGMacs populate the DRG after nerve injury, and include self-renewing macrophages, microglia-like cells, and Imoonglia.

Locally Proliferating DRG Macrophages Contribute to Promote Axon Regeneration. To determine which type of DRGMacs contribute to regulate axon regeneration, we first determined if continuous PLX treatment (14 d before injury and 3 d after injury) deplete a specific subtype using lineage tracing. To label macrophages, one group of *Cx3cr1*^{CreER}::Ai14 mice was treated with TAM at 4 wk of age (4-wk-old TAM). To label microglia-like cells, another group of *Cx3cr1*^{CreER}::Ai14 was treated with a TAM at E9.5 (E9.5 TAM). To label Imoonglia, a group of *Fabp7*^{CreER}::Ai14 was treated with TAM at 4 wk of age. All mice were injected with BrdU once daily for 3 d right after nerve injury to label proliferating cells (*SI Appendix*, Fig. S4*A*). We then counted the number of IBA1 and tdTomato-positive cells, which were or not labeled with BrdU in the continuous PLX treatment group compared with PLX+CD in each of the three tracing groups. We observed that continuous PLX treatment after nerve injury decreased the number of IBA1/tdTomato/BrdU-positive cells in *Cx3cr1*^{CreER}::Ai14 (4-wk-old TAM), indicating that self-renewal of DRGMacs was impaired (Fig. 3*A* and *SI Appendix*, Fig. S4*B*). In contrast, the number of tdTomato/IBA1-positive cells that were BrdU negative was not altered in all other conditions (Fig. 3*A* and *SI Appendix*, Fig. S4 *C* and *D*). These results suggest that continuous PLX treatment affects macrophage repopulation by preventing the proliferation of DRGMacs after injury but does not alter microglia-like cells and Imoonglia.

DRGMacs have been shown to enhance the regenerative capacity of sensory neurons (18, 19) in the conditioning injury paradigm, in which a prior nerve injury increases the growth capacity of sensory neurons (1). However, which subtypes of macrophage are responsible for this effect is unclear. We thus determined if impairing DRGMac self-renewal without affecting the other DRGMac populations with continuous PLX treatment impacts the extent of axon regeneration in vivo and in vitro. Since macrophages also regulate nerve repair at the site of injury, we first tested if PLX treatment affected macrophage recruitment in the nerve. We observed no differences in the percent of IBA1-positive cells in the injured nerve between treatment groups (Fig. 3 *B* and *C* and *SI Appendix*, Fig. S4 *E*–*J*), indicating that while PLX treatment depleted resident macrophages in the nerve (*SI Appendix*, Fig. S1*E*), it did not affect macrophage recruitment at the site of nerve injury. These results are consistent with previous reports that macrophages in the nerve mostly derive from recruited bone-marrow–derived precursors (12, 13, 26).

To examine whether preventing DRGMac self-renewal impairs axon regeneration in vivo, we quantified axon regeneration 3 d post SNC in three groups of mice, CD (CD+CD), PLX treatment

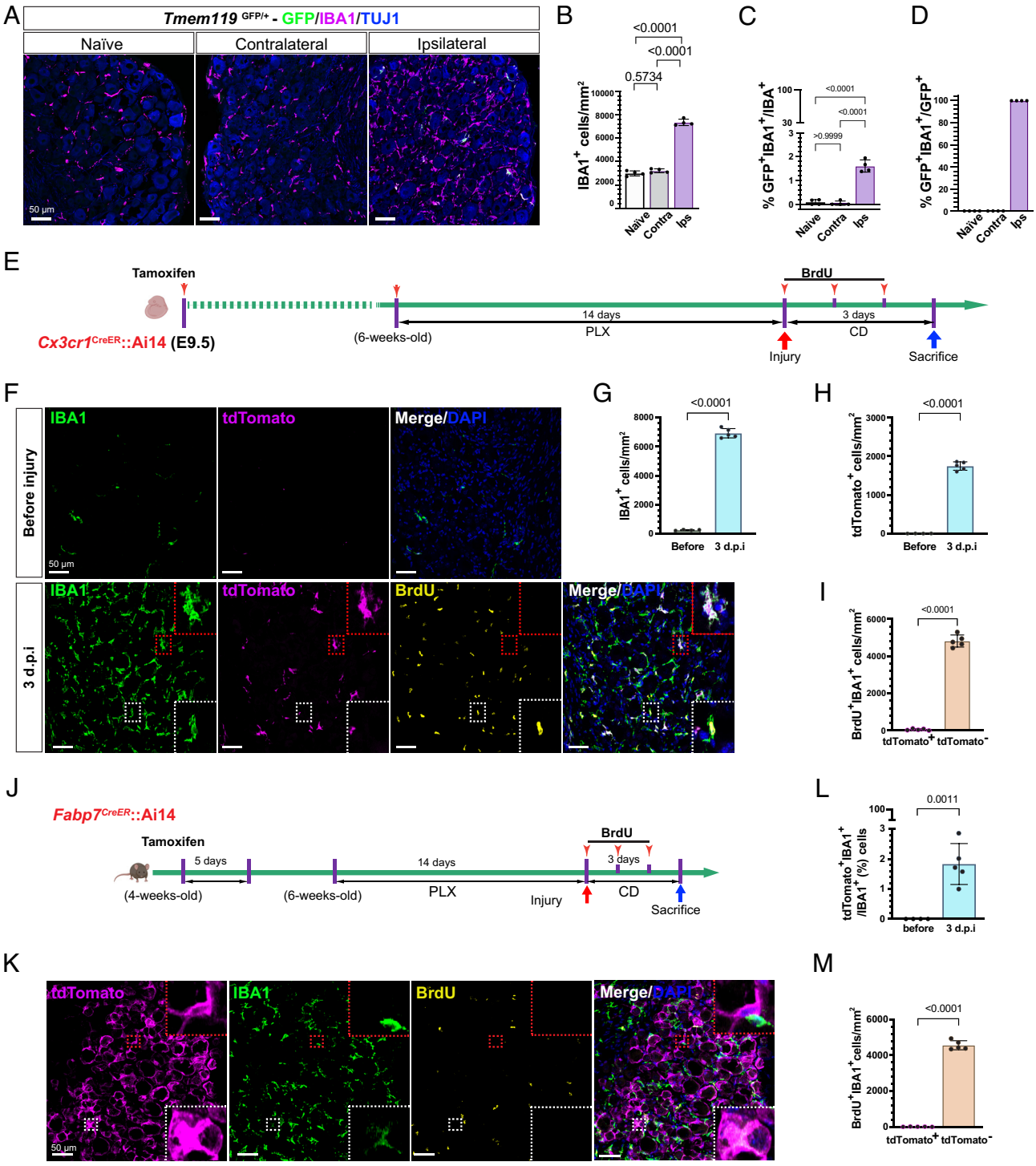

Fig. 2. Two small subsets of cells repopulate in DRGMacs after nerve injury. (*A*) Representative images of DRG sections 3 d after SNC in *Tmeme119*$^{GFP/+}$ mice, stained for GFP (green), TUJ1 (neurons, blue) and macrophages (IBA1, magenta) in the indicated condition. (Scale bars, 50 µm.) (*B–D*) Quantification of IBA1$^+$ cells (*B*), percentage of GFP$^+$IBA1$^+$ cells in IBA1$^+$ cells (*C*) and percentage of GFP$^+$IBA1$^+$ cells in GFP$^+$ cells (*D*) in the naive, contralateral and ipsilateral DRGs 3 d post injury. N = 4 in each condition. (*E*) Scheme of CNS microglia fate mapping after sciatic nerve injury using *Cx3cr1*^{CreER}::Ai14 mice and a single tamoxifen treatment at E9.5. (*F*) Representative images of DRG sections from E9.5 tamoxifen-treated *Cx3cr1*^{CreER}::Ai14 mice before and 3 d after sciatic nerve injury, with a prior 14 d period of PLX treatment. (Scale bars, 50 µm.) (*G* and *H*) Quantification of IBA1$^+$ cells/mm^2(*G*), tdTomato$^+$ cells/mm^2 (*H*) in the DRG sections. N = 4 (before injury) and 5 (3 d.p.i), respectively. (*I*) Quantification of BrdU$^+$IBA1$^+$ incorporated with tdTomato$^+$ or tdTomato$^-$ cell density (cells/mm^2) in DRG sections. (*J*) Scheme of SGCs fate mapping after PLX treatment using *Fabp7*^{CreER}::Ai14 mice. (*K*) Representative immunostaining images of DRGs from PLX treated mice 3 d after SNC, showing tdTomato (magenta), IBA1 (green), BrdU (yellow), and DAPI (blue). Higher magnification images from white/red boxed areas was showed in the corner of each image, (scale bar, 50 µm.) (*L*) Quantification of the percentage of tdTomato$^+$IBA1$^+$ cells in IBA1$^+$ cells in the DRGs of *Fabp7*^{CreER}::Ai14 mice before and at 3 d after SNC with period of PLX treatment. N = 4 (before injury) and 5 (3 d.p.i), respectively. (*M*) Quantification of BrdU$^+$IBA1$^+$ incorporated with tdTomato$^+$ or tdTomato$^-$ cell density (cells/mm^2) in the DRGs of *Fabp7*^{CreER}::Ai14 mice at 3 d after SNC with period of PLX treatment. N = 5. The data are presented as mean ± SD. N presented mouse number.

(PLX+CD), and continuous PLX treatment (PLX+PLX). The extent of axon regeneration past the injury site was measured by labeling nerve sections with SCG10, a marker for regenerating axons (49). The highest SCG10 intensity along the nerve was defined as the crush site, as described (49, 50). The length of the 10 longest axons reflects the extent of axon elongation, regardless

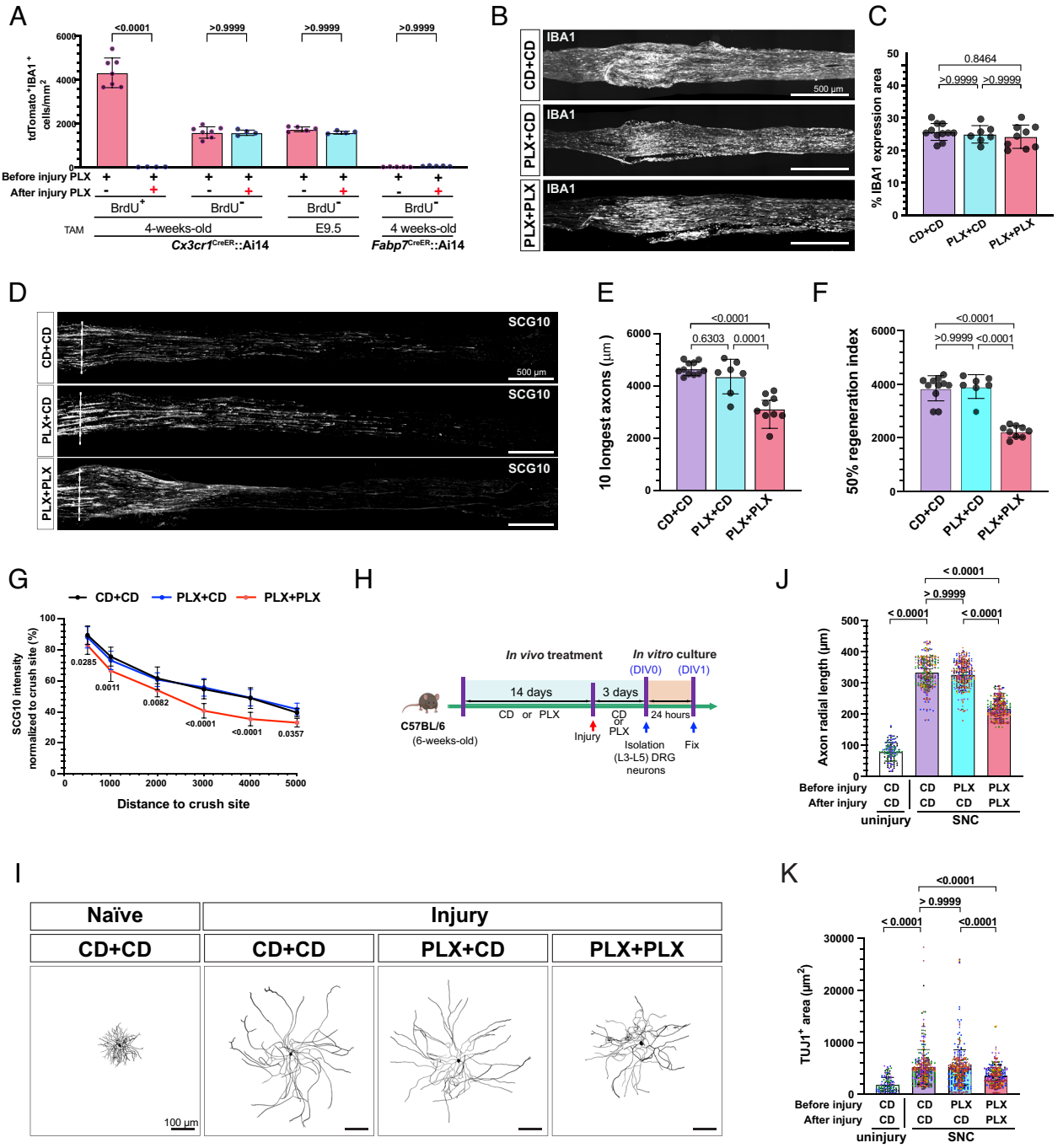

Fig. 3. DRG macrophages contribute to promote axon regeneration. (*A*) Quantification of the density of tdTomato^{+}IBA1 cells with or without BrdU in the DRGs using multiple tracing methods, with or without continues PLX treatment after injury. N (mouse number) = 7 (PLX+CD, 4-wk-old TAM *Cx3cr1*^{CreER}::Ai14), N = 4 (PLX+PLX, 4-wk-old TAM *Cx3cr1*^{CreER}::Ai14), N = 5 (PLX+CD, E9.5 TAM *Cx3cr1*^{CreER}::Ai14), N = 4 (PLX+PLX, E9.5 TAM *Cx3cr1*^{CreER}::Ai14), N = 5 (PLX+CD, 4-wk-old TAM *Fabp7*^{CreER}::Ai14) and N = 5 (PLX+PLX, 4-wk-old TAM *Fabp7*^{CreER}::Ai14). (*B*) Representative images of sciatic nerve 3 d after SNC immune-stained from IBA1 and mice with the indicated treatment. (Scale bars, 500 µm.) (*C*) Quantification of the IBA1^{+} area expression area in the distal stump of regenerating sciatic nerve between treatment groups. N (mouse number) = 11 (CD+CD), N = 7 (PLX+CD) and N = 9 (PLX+PLX), respectively. (*D*) Representative longitudinal sections of sciatic nerves 3 d after SNC immunostained for SCG10 from mice with the indicated treatment. Dotted line indicates the crush site, determined as the maximal SGC10 intensity. (Scale bars, 500 µm.) *(E-G)* Length of the 10 longest axons was measured (*E*) length distinct in 50% regeneration index was measured as the SGC10 intensity in the distance to the crush site normalized to the crush site for 50% (*F*), regeneration index was measured as the SGC10 intensity normalized to the crush site for a given distance to the crush site (*G*) between conditions. N (mouse number) = 11 (CD+CD), 7 (PLX+CD) and 9 (PLX+PLX) in female mice, respectively. (*H*) Scheme of adult DRG neuronal culture in naive, CD or PLX diet-treated mice. (*I*) Representative images showing TUJ1 (black) immunostaining in adult DRG neurons cultured for 24 h. (Scale bars, 100 µm.) (*J* and *K*) Quantification of axonal radial length (*J*) and axon growth capacity (*K*). Different colors represent different biological replicates. N (neuron number) = 154 (CD+CD; four biological replicates, naive mice), 460 (CD+CD; six biological replicates, injured mice), 468 (PLX+CD; six biological replicates, injured mice) and 465 (PLX+PLX; six biological replicates, injured mice), respectively. The data are presented as mean ± SD.

of the number of axons that regenerate (51). The regeneration index obtained by normalizing the average SCG10 intensity at distances away from the crush site to the SCG10 intensity at the crush site take into account both the length and the number of regenerating axons past the crush site (50). We found that axon regeneration was similar in PLX-treated mice (PLX+CD) and control mice (CD+CD) (Fig. 3 *D*–*G*). However, axon regeneration was reduced in mice with continuous PLX treatment (PLX+PLX) compared with control mice (CD+CD). This impairment of axon regeneration is modest, and consistent with the

notion that intrinsic mechanisms in the injured neuron and in the surrounding SGC promote axon regeneration (5, 52). The same treatments and measurements were performed in both male and female mice, and no significant differences were observed (*SI Appendix*, Fig. S5 *A* and *B*). These results indicate that self-renewing DRGMacs and possibly resident macrophages in the nerve contribute to promoting axon regeneration in the earlier stage after injury in a gender-independent manner.

To further determine whether self-renewing DRGMacs affect the regenerative capacity of DRG neurons, we tested if PLX treatment impaired the conditioning injury paradigm. We purified DRG neurons from mice with or without PLX treatment as described above, and cultured them for 24 h (Fig. 3*H*). For quantification of neuron growth capacity, neurons were immunostained for TUJ1, and radial length was measured (Fig. 3*I*). We also measured the TUJ1-positive area by neurite tracing using "Simple Neurite Tracer" plug-in in Fiji (Fig. 3*J*). As expected, a prior injury 3 d before collecting DRG led to improved axon growth capacity, revealed by longer neurites and increased TUJ1 staining area in the control group (CD+CD) (Fig. 3 *I* and *J*). Treatment with PLX prior to injury (PLX+CD) did not affect the injury-induced increased growth capacity of DRG neuron (Fig. 3 *I* and *J*). However, continued PLX treatment (PLX+PLX) reduced axon growth capacity compared with CD+CD or PLX+CD (Fig. 3 *I* and *J*). The conditioning effect was not completely blocked, consistent with the notion that transcriptional and epigenetic changes in the injured neurons controls the mode of axon growth after injury (1, 5, 53). To exclude the possibility of a direct effect of PLX on neurons and their axon growth capacity, axon growth was compared in uninjured contralateral (CON) and naive DRGs treated with CD or PLX. Similar growth capacity was observed in all conditions (*SI Appendix*, Fig. S5 *C* and *D*), indicating that PLX treatment does not directly impact neurons. This is consistent with the observation that Csf1r is not expressed in sensory neurons (7, 54). The same treatments and measurements were performed in both male and female mice and no significant differences were observed (*SI Appendix*, Fig. S5 *E* and *F*). Together, these results indicate that macrophage self-renewal in the DRG and possibly resident macrophages in the nerve contribute to promote axon regeneration in the early stage after nerve injury.

Communications between Macrophages and Other Cell Types after Nerve Injury. To gain further insights into the molecular mechanisms by which DRGMacs regulate axon regeneration, we performed single-cell RNA seq to compare the injury responses of DRGMacs in normal diet conditions (Normal diet) and in the PLX+CD diet group (PLX diet), in which repopulated DRGMacs support axon regeneration to the same extent as normal diet (Fig. 3 *D*–*J*). As a normal diet, we used our previously generated dataset, 3 d post SNC (9). scRNA-seq was performed on injured (SNC) and CON DRG from mice treated with PLX+CD using the chromium single-cell gene expression solution (10 X Genomics). The number of total sequenced cells from two biological replicates was 10,311 with an average of 85,332 reads per cell, 2,068 genes per cell, and an average of total of 20,426 genes per sample detected. In both groups, mice were of the same age, gender, and the same procedure and filtering criteria were used (see filtering criteria in the methods). The PLX diet and normal diet samples were pooled and an unbiased (Graph-based) clustering, using Partek flow analysis package, identified 23 distinct cell clusters (*SI Appendix*, Fig. S6*A*). To identify cluster-specific genes, we calculated the expression difference of each gene between that cluster and the average in the rest of the clusters (ANOVA fold change threshold >2, resource data related to Fig. 4). Examination of the cluster-specific marker genes revealed major cellular subtypes including connective tissue cells (*Col1a1*), T cells (*Cd3g*), Schwann cells (*Ncmap*), SGC (*Fabp7*), neurons (*Isl1*), endothelial cells (*Pecam1*), pericytes (*Mcam*), and macrophages (*Aif1*(IBA1); *Cd68*) (*SI Appendix*, Fig. S6 *B*–*J*, resource data related to Fig. 4). Our scRNAseq protocol achieves efficient recovery of nonneuronal cells only and thus is not suitable for in-depth analysis of neuronal responses (9, 52).

The macrophage clusters were pooled for analysis. We observed that the repopulated DRGMacs clusters (PLX diet) were distinct from DRGMacs in normal diet, highlighting distinct transcriptional profiles (Fig. 4*A*). This is similar to repopulated microglia in the brain, which also display distinct transcriptional profiles compared with resident microglia (34). Injury did not dramatically affect macrophage clustering in either PLX diet or normal diet (Fig. 4*A*). To define the transcriptional response of macrophages to nerve injury, cells in the macrophages cluster were pooled in normal diet or PLX diet, control and injury conditions were compared to identify differentially expressed (DE) genes after injury (Fig. 4*B*). We found that only 45 up-regulated and 17 down-regulated genes after injury were common between normal diet and PLX diet treatment (Fig. 4*C*). Kyoto Encyclopedia of Genes and Genomes (KEGG) analysis did not return any significant pathway enrichment for these shared genes.

To further understand the mechanisms by which DRGMacs support axon regeneration, we analyzed cell–cell communication with CellChat (55). The number of incoming interaction and outgoing interactions in each cluster was analyzed in each condition. DRGMacs display higher incoming signaling strength compared with outgoing signaling strength in all conditions (*SI Appendix*, Fig. S6*K*), suggesting that DRGMacs act mostly as receivers in the DRG microenvironment. SGCs showed the highest strength of signaling in both incoming and outgoing interactions (*SI Appendix*, Fig. S6*K*). We next determined which signaling pathways are involved in DRGMacs communication in the DRG microenvironment after nerve injury. The significant signaling pathways active in the DRG microenvironment were identified (*SI Appendix*, Fig. S7 *A* and *B*). This analysis revealed that seven incoming pathways participate in DRGMacs communication after SNC in normal diet and PLX diet treatment (Fig. 4*D*). These include APP, macrophage-colony stimulating factor (CSF), GALECTIN, intercellular adhesion molecule (ICAM), melanocyte release inhibiting factor, COMPLEMENT and CCL. Only one outgoing pathway PSAP (Prosaposin) was identified (Fig. 4*D*).

We then compared the communication probabilities from cell–cell clusters in these signaling pathways. Macrophages act as the major receivers from multiple cell types in APP signaling, from endothelial cells in GALECTIN and ICAM pathways, and from pericyte in CSF signaling pathway (Fig. 4*E* and *SI Appendix*, Fig. S7*C*). Macrophages act both as sender and receivers in the CCL signaling pathway (*SI Appendix*, Fig. S7*C*). Previous studies suggested that CCL2 expression in neurons could function to recruit CCR2-positive monocytes after injury or lead to stimulation of macrophages (19, 20). Since we recovered only few neurons in our single-cell data sets, we are unable to analyze CCL signaling between neurons and macrophages in depth. However, we observed that CCL6-CCR1 contributed to ligand–receptor pair in the CCL signaling after SNC in both normal diet and PLX diet treatment (*SI Appendix*, Fig. S7*C*), albeit between different cell types in PLX and normal diet.

Interestingly, the PSAP (Prosaposin) signaling pathway is the only outgoing signaling from macrophages in both normal diet and PLX diet treatment, with SGCs acting as the major PSAP signaling receiver (Fig. 4*E*). We then analyzed the ligand–receptor pairs that are highly relevant in macrophage–SGC interaction in normal diet and PLX diet treatment after SNC (Fig. 4*F*). PSAP in macrophage

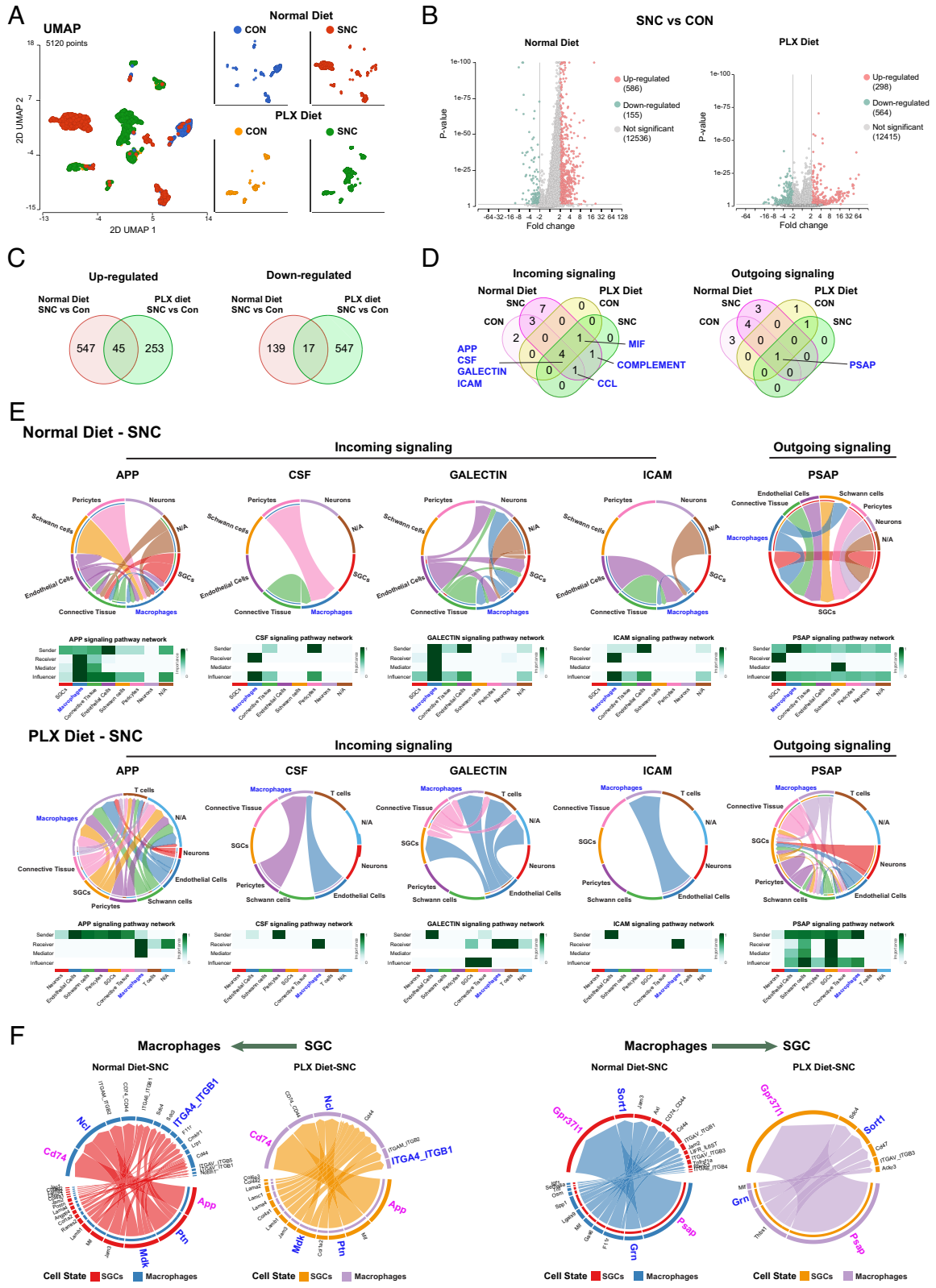

Fig. 4. Cell communications between macrophages and other cell types in DRG. (*A*) UMAP of transcriptional profiles of macrophage in the control side (CON) and injured side (SNC) of DRGs at 3 d post injury with either normal diet or PLX diet treatment period of injury. N (cell number) = 820 (Normal diet-CON), 1,779 (Normal diet-SNC), 509 (PLX diet-CON), 2,012 (PLX diet-SNC), respectively. (*B*) Volcano plot showing DEGs (FDR < 0.05 and |fold-change| > 2) between macrophage with injured (SNC) and control (CON) sides of DRGs at 3 d.p.i. under normal diet (*Left*) and PLX diet (*Right*) treatment period of SNC. The numbers of DEGs are indicated in parentheses. (*C*) Venn diagram of up-regulated (*Left*) and down-regulated (*Right*) DEGs between injured to control under normal diet treatment was compared with PLX diet treatment. (*D*) Venn diagram of incoming (*Left*) and outcoming (*Right*) signalings in DRGMacs in the control side (CON) and injured side (SNC) of DRGs at 3 d post injury with either normal diet or PLX diet treatment period of injury. (*E*) Chord diagram inferred the APP, CSF, GALECTIN, ICAM macrophage incoming signaling and PSAP macrophage outgoing signaling under normal diet treatment (*Upper*) or PLX diet treatment (*Bottom*) in SNC reconstructed with CellChat. The size of the width of various colors in the periphery indicates probability/intensity value of interaction (intensity is the sum of probability values). Heatmaps quantify the role of each cluster as a sender, receiver, mediator, and influencer. (*F*) Chord diagram inferred the legend–receptor pairs between macrophage and SGC under normal diet treatment or PLX diet treatment in SNC reconstructed with CellChat. SGCs to macrophages (*Left*); macrophage to SGCs (*Right*). The size of the width of various colors in the periphery indicates probability/intensity value of interaction (intensity is the sum of probability values).

and GPR37L1 in SGC were the major ligand–receptor pairs underlying macrophage to SGC communication, followed by progranulin-Sortilin1 (Fig. 4*F*). Prosaposin- and prosaposin-derived peptides are ligands of GPR37 and GPR37L1 and exhibit neuroprotective, glioprotective, and analgesic effects (56–60). We found that GPR37-PSAP was a major contributor in the communication between macrophages and endothelial cells (*SI Appendix*, Fig. S8*A*). Nearly all SGCs expressed *Gpr37l1,* whereas only few SGCs expressed *Gpr37* (*SI Appendix*, Fig. S8*B*). *Psap* was highly expressed in a majority of DRGMacs (*SI Appendix*, Fig. S8*B*). To validate the predicted macrophage-SGC communication via PSAP-GPR37L1 signaling, we prepared DRG explants from mice treated with PLX, in which most macrophages were depleted. Explants were then treated with either vehicle or 10 nM Prosaptide Tx14(A) (here after referred to as TX14), which was shown to bind GPR37 and GPR37L1 and activate ERK (58). We examined the level of ERK phosphorylation and observed that TX14 induced ERK phosphorylation in some SGCs (*SI Appendix*, Fig. S8 *E* and *F*)). TX14 also enhanced neurite outgrowth from the explant, (*SI Appendix*, Fig. S8 *G*, *H*, and *I*), consistent with previous reports showing that TX14 can improve aspects of nerve regeneration (60). These results support a functional role of PSAP-GRP37/GPR37L1 in cell–cell communication in the DRG revealed by the cell chat analysis. We did not observe changes in the expression level of *Psap* or GPR37L1 after SNC in our single-cell data, but this does not exclude the possibility that this signaling pathway is regulated by injury at a posttranscriptional level, since prosaposin secretion correlates with nerve regeneration capacity (60). Together, this analysis suggests that macrophages express the neuroprotective and glioprotective ligand prosaposin and communicate with SGCs via the prosaposin receptor GPR37L1 and with endothelial cells via GPR37 (*SI Appendix*, Fig. S8*J*).

Discussion

DRGMacs have been implicated in nerve regeneration (18–20) and in nerve injury-induced pain (22, 61). However, the source and function of DRGMacs in nerve injury responses have remained unclear. We report here that four different populations of macrophages populate the DRG after nerve injury. These results will pave the way for a better understanding of the immune mechanisms governing pain and nerve repair after injury and other peripheral neuropathies.

Macrophages in all tissues adapt to their environment and are strongly imprinted by their tissue of residence (62, 63). Macrophages broadly consist of two classes: tissue-resident macrophages and infiltrating macrophages. After peripheral nerve injury, macrophages in the injured nerve expand as a result of infiltrating macrophages, which mainly derive from circulating bone-marrow–derived precursors (11–14). Previous studies also reported an increase in the number of DRGMacs after peripheral nerve injury (9, 17, 19, 22, 26), but whether macrophage accumulation is the result of recruitment or local proliferation has remained unclear. We established a macrophage depletion model and took advantage of multiple genetic mouse models to trace macrophages (33), microglia (38), and SGCs (43). This approach allowed us to investigate the source of DRGMacs in response to peripheral nerve injury. We found that four populations of macrophages reside in the DRG at an early stage after nerve injury. Self-renewing macrophages, proliferating from local resident macrophages, represent the largest population of DRGMacs, and this population contributes to promote axon regeneration. Our results suggest that after depletion, macrophages rapidly replenish the DRG. This is similar to the situation in the brain, in which microglia depletion is followed by a rapid proliferation and replenishment of the microglia density to normal levels (34). This was attributed to residual microglia in the brain repopulating with fast proliferative kinetics compared with resident microglia during the first 2 d after PLX removal (34). Our results parallel these findings, as we observed more DRGMac self-proliferation after PLX removal compared with the normal diet situation.

In addition to self-renewing macrophages, we also found that microglia-like cells populate the DRG after nerve injury. Microglia-like cells and proliferating macrophages may play distinct roles after nerve injury. In the injured nerve, macrophages express features of microglia (12). It is thus possible that the microglia-like cells we observed in the DRG represent a similar population of microglia-like macrophages. Another possibility, which is supported by our microglia tracing experiment, is that microglia migrate from the dorsal horn along dorsal root axons to reach the DRG. This scenario is consistent with the high migratory activity of microglia in the brain (64) and has been observed in zebrafish, in which dorsal root avulsion injury elicits microglia exit from the spinal cord (37). In this model, the traveling microglia clear debris at the injury site and carry that debris back into the CNS (37). In our assay, the injury site is further away in the nerve. Whether microglia-like cells can reach the injury site in the nerve and perform similar functions as those observed in the zebrafish remains to be tested. A more likely function may be related to pain. Indeed, DRG macrophages (22) and microglia in the spinal cord (65) were shown to contribute to neuropathic pain after nerve injury. After nerve injury, activation and accumulation of microglia occurs in the dorsal horn, where dorsal root axons enter the spinal cord (65, 66). The detailed function and mechanism by which microglia-like cells populate the DRG need to be further investigated.

Our lineage tracing experiment also indicates that a subpopulation of DRGMacs is macrophage-like SGCs, consistent with our previous identification of Imoonglia, a cell type that is increased after injury, which express macrophage genes and shares the spatial arrangement of SGCs surrounding sensory neurons. This is consistent with the notion that SGCs express progenitor markers, such as Sox2, Foxd3, Nestin, and p75, and thus have the potential to differentiate into other cells (9, 67). The detailed mechanism by which a subset of SGCs express macrophage genes after injury and whether this population evolves at later time point during the course of regeneration will require future investigation. Our previous study indicates that these cells increase in number after both peripheral and central axon injuries (9). Gene ontology analysis of Imoonglia suggests an immune function, with enrichment for chemokine–cytokine signaling and Toll-like receptor signaling (9). In human trigeminal ganglion, SGCs were shown to express Toll-like receptors (68), suggesting that Imoonglia may play a role in initiating and orchestrating inflammation responses.

Our study provides the identification of multiple DRGMac origins three days post nerve injury. It has been shown that the number of macrophages populating the DRG increase by days 3 and 7 after nerve injury. Whether they return to the basal level by day 14 or 28 post injury remains to be confirmed (18, 26). Future studies are needed to determine how the distinct subpopulation of DRGMacs evolve in time, which may inform future therapeutic approaches to treat nerve injury to promote recovery without pain.

Imprinting by the tissue environment has been suggested to be the dominant factor conferring macrophage identity and self-maintenance capacity (69). Depleting macrophages may have changed the DRG environment, and that is reflected by the distinct transcriptional signature we observed between macrophages and repopulated macrophages at the single-cell level. This raises the possibility that repopulated macrophages function differently compared with normal macrophages after nerve injury. However, since repopulated DRGMacs supported axon regeneration to the same extent as

DRGMacs in normal conditions, we focused our analysis on the common pathways between the two conditions. We thus performed single-cell data RNAseq and analyzed the transcriptional response of DRGMacs after nerve injury in control and repopulated conditions. Although overall, the transcriptional signature of DRGMacs and repopulated DRGMacs was distinct, as expected, some cell–cell interaction networks appeared to be conserved in normal and repopulated conditions. Notably, we found that DRGMacs express the neuroprotective, glioprotective, and analgesic ligand prosaposin (56–59), suggesting that they communicate with SGC via the prosaposin receptor GPR37L1, and may provide some level of glioprotection. It was recently reported that a small number of SGC undergo apoptosis after axotomy (70), in addition to the known neuronal death induced by nerve injury (71). Prosaposin is known to protect myelinating glia cells, promoting Schwann cell survival in the face of cellular insults and to increase expression of enzyme important for myelination (56). Mechanistically, ERK phosphorylation in SGC may depend on prosaposin secretion from DRGMacs, since prosaptide stimulation of GPFR37L1 was shown to induce the phosphorylation of ERK (58), and nerve injury leads to phosphorylation of ERK in SGC in addition to neurons (72).

In conclusion, we demonstrated that four subpopulations of macrophages populate the DRG after nerve injury, including local self-renewing macrophages, microglia-like macrophages, and Imoonglia in addition to a small population of circulating bone-marrow–derived precursors. The self-renewing population contributes to promote axon regeneration. The precise function of the other subtypes of DRG macrophages after nerve injury remains to be determined. Future studies aimed at harnessing the different DRGMacs origin may inform future therapeutic approaches to treat nerve injuries.

Materials and Methods

Experimental Model and Subject Details. Two-month-old female and male C57BL/6 mice, *Cx3cr1*^{CreER} x Ai14 (*Cx3cr1*^{CreER}::Ai14), *Tmem119*$^{GFP/+}$, *Blbp*^{CreER} x Ai14 (*Blbp*^{CreER}::Ai14) mice were used in this study. Mouse colonies were bred and maintained in temperature (64 to 79°F) and humidity control (30 to 70%) in Washington University in St. Louis animal facility. Mice were housed socially (1 to 5 mice per cage) on a 12–h light/dark cycle (6am/6pm) in individually ventilated cages and with ad libitum access to food and water. Littermates of the same gender were otherwise randomly assigned to experimental groups. All experiments were conducted in accordance with the protocol (21-0104) approved from Institutional Animal Care and Use Committees (IACUCs) of Washington University in St. Louis.

Animals. All animals were approved by the Washington University School of Medicine IACUC under protocol A-3381-01. All experiments were performed in accordance with the relevant guidelines and regulations. Mice were housed and cared for in the Washington University School of Medicine animal care facility. This facility is accredited by the Association for Assessment & Accreditation of Laboratory Animal Care and conforms to the PHS guidelines for Animal Care. Accreditation–7/18/97, USDA Accreditation: Registration # 43-R-008. Wild-type C57BL/6 mice were obtained from Envigo (Envigo #027) and Jackson Laboratory (Stock No: 000664). *Cx3cr1*^{CreER} (33) (B6.129P2(C)-*Cx3cr1*$^{tm2.1(cre/ERT2)Jung}$/J, JAX Stock No: 020940), Ai14 (73) (B6.Cg-Gt(ROSA)$^{26Sortm14(CAG-tdTomato)Hze}$/J, JAX Stock No: 007914) *Tmem119*$^{GFP/GFP}$ (38) (C57BL/6-$^{Tmem119em2(EGFP)Gfng}$/J, JAX Stock No: 301823) mice were obtained from The Jackson Laboratory. The *Blbp*^{creER} (43) mouse line was a generous gift from Dr. Toshihiko Hosoya. Ai14 mice were crossed with *Cx3cr1*^{CreER}, and *Blbp*^{CreER} mice to obtain *Cx3cr1*^{CreER}::Ai14 and *Blbp*^{CreER}::Ai14 mice. *Tmem119*$^{GFP/+}$ knock-in mice were obtained by crossing *Tmem119*$^{GFP/GFP}$ and C57BL/6 J mice. All animals were housed on a 12/12 light–dark cycle with food and water ad libitum.

Primary Adult DRG Neuronal and Explant Culture. L4 and L5 DRGs from 8-wk-old mice were collected into cold dissection medium [Hanks' Balanced Salt Solution (HBSS) (Thermofisher, Gibco; Catalog#:14175-079)] with 10% 1M HEPES [(Thermofisher, Gibco); Catalog#15630080], then transferred to fresh made prewarmed dissociation medium (15U/mL Papain suspension (Worthington Biochemical; Catalog#LS003126), 0.3 mg/mL L-cysteine (Sigma; Catalog#C7352), 0.1 mg/mL Deoxyribonuclease I (Worthington Biochemical; Catalog#LS002139), 10% 1M HEPES in HBSS) incubated in 37 °C for 20 min. Samples were incubated with collagenase (150 μg/mL; Sigma; Catalog#C6885) in 37 °C for 20 min after washing with prewarmed HBSS twice. After washing with prewarmed HBSS twice, the single-cell suspension was resuspend by gently triturating in complete medium (Neurobasal™-A Medium, Thermofisher, Gibco; Catalog# 12349015) with B-27™ Plus Supplement [Thermofisher, Gibco; Catalog# A3582801; GlutaMAX™ Supplement (Thermofisher, Gibco; Catalog#35050061)]. Afterward, the single-cell suspension was carefully added on Percoll (Sigma, Catalog# P1644) mixture (3 mL 60% Percoll overlay with 3 mL 30% Percoll for one condition in a 14-mL round bottom tube). Next, the samples were centrifuged at 800 × rpm at 4 °C for 20 min. The neuron layer was carefully collected and put in 10 mL HBSS with 10% HEPES. The samples were centrifuged at 500 × rpm at 4 °C for 5 min. The cell pellet was resuspended in complete neurobasal medium. Cells were seeded on PDL/laminin-coated 18-mm coverslips with cell density as 1.0×10^3/coverslip.

For adult DRG explant culture, L4 DRGs from 8-wk-old mice were collected into cold dissection medium [HBSS (Thermofisher, Gibco; Catalog#:14175-079)] with 10% 1M HEPES (Thermofisher, Gibco; Catalog#15630080) and 18 mM D-Glucose (Sigma; Catalog# G7021). DRGs were then seeded on PDL/ laminin-coated eight Chamber cell culture slides (Celltreat, Catalog#229168) with 10 nM Prosaptide T×14(A) (MedChemExpress; Catalog# HY-P1342) or 0.1%DMSO in complete medium (Neurobasal™-A Medium, Thermofisher, Gibco; Catalog# 12349015) with B-27™ Plus Supplement (Thermofisher, Gibco; Catalog# A3582801); GlutaMAX™ Supplement (Thermofisher, Gibco; Catalog#35050061), and 2.5% Fetal Bovine Serum (FBS) (Gibco, Catalog#A31604).

Sciatic Nerve Injury. Sciatic nerve injuries were performed as previously described (2, 50, 52). During surgery, 8-wk-old mice were anesthetized using 1.5% inhaled isoflurane. The sciatic nerve was exposed at the mid-thigh level (around 1.2 cm to L4 DRG) with a small skin incision. The sciatic nerve was fully crushed for 10 s with 0.1-mm forceps (#55). The wound was closed using wound clips. Mice were placed on a warming pad after surgery until fully awake. L4 and L5 DRG were dissected at the indicated time postsurgery.

Drug Administration. To pharmacological ablate DRG macrophage, mice were fed PLX73086-formulated AIN-76A diet (200 mg PLX73086 per kilogram of diet, Plexxikon, Research Diet) or PLX5622-formulated AIN-76A diet (1,200 mg PLX73086 per kilogram of diet, Plexxikon, Research Diet) ad libitum. Mice were fed normal AIN-76A diet (Plexxikon, Research Diet, Cat#D10001i) as control. To efficiently induce the CreER-dependent recombination, tamoxifen (Sigma, T5648; Log# WXBD2299V) dissolved in corn oil (Sigma, Catlog#C8267, Log#MKCK6411) was oral gavage administered to mice with tamoxifen daily at 100 mg/kg body weight for five consecutive days. To induce expression of tdTomato in YSMacs, 100 mg/kg tamoxifen and 37.5 mg/kg progesterone (Merck, Catalog#P0130) dissolved in corn oil were given by oral gavage to pregnant females carrying *Cx3cr1*^{CreER}:Ai14 embryos at E9.5.

BrdU Labeling. BrdU (Abcam, Catlog#ab142567) was dissolved in DPBS at a concentration of 10 mg/mL and was administered by intraperitoneal injection to mice. Using a 3-d loading protocol, BrdU was given immediately after injury and once daily for three consecutive days at 100 mg/kg. Mice were killed 24 h after the last BrdU injection.

Quantitative Real-Time PCR. For qRT-PCR, L4 and L5 DRGs of each mouse were collected and total RNA was extracted using RNeasy Mini Kit (QIAGEN, Cat# 74104). For copy DNA (cDNA) synthesis, 500 ng RNA was converted into cDNA with the High-Capacity cDNA Reverse Transcription Kit (ThermoFisher, Catlog# 4368814) according to the manufacturer's specifications. Quantitative PCR was completed using the PowerUp™ SYBR™ Green Master Mix (ThermoFisher, Cat# A25780) using gene-specific primers (resource table) from Primerbank (https://pga.mgh.harvard.edu/primerbank/). qRT-PCR was performed on a QuantStudio six Flex System. Expression fold change for each gene of interest was calculated using the ΔCq method and normalized to the expression fold change of *Gadph* expression compared with controls.

Immunohistochemistry. Mice were killed with CO_2 asphyxiation and transcardially perfused with phosphate-bufferedsaline (PBS) followed by 4% paraformaldehyde (PFA). PFA-fixed tissues were incubated in 30% sucrose in PBS overnight at 4 °C, specimens were embedded in optimal cutting temperature compound

(Tissue-Tek), stored at −80 °C until further processing. Transverse sections of DRG (L4) and longitudinal sections of sciatic nerve were cut on a cryostat at 10 μm, transverse sections of spinal cord (L4) were cut on 25-μm thickness and stored at −20 °C until processed. Before staining, sections were warmed to room temperature and dried on a 60 °C slide warmer for 5 min. For detecting of BrdU-labeling cells, the slides were rinsed in DPBS, denatured in 2N HCl for 30 min, rinsed in PBS, then following general immunohistochemistry protocol. Sections were treated with a blocking solution containing 4% normal donkey serum (NDS) (LAMPIRE; Catalog#7332100) with 0.5% Triton X-100 in PBS for 1 h at room temperature. Then samples were incubated in the primary antibodies, which were diluted in 1% NDS with 0.3% Triton X-100 in PBS overnight at 4 °C. After three PBS rinses, samples were incubated with Alexa Fluor–conjugated secondary antibodies in PBS with 0.3% Triton X-100 in 1 h, followed by incubation in 300 nM DAPI (Sigma-Aldrich, Catalog# D9542) at room temperature for 10 min. Samples were rinsed before mounting with ProLong™ Gold Antifade Mountant (Invitrogen, Catalog#:P36930). DRG sections were imaged with a confocal laser-scanning microscope (Zeiss LSM880). Figures showing large longitudinal sciatic nerve sections, stitched spinal cord and brain sections were produced using EVOS™ M7000 Imaging System with image stitching and/or stack software. For adult DRG neuronal culture and DRG explant culture staining, neurons/explants were fixed in prewarmed 1%PFA in 7.5% sucrose at 37 °C for 15 min. Then postfixed in prewarmed 2%PFA in 15% sucrose in 30 min. Rise with PBS 3 times, the fixed neurons were directly for immunostaining following same staining protocol described above. Cultured neurons were imaged using the ECLIPSE Ti2 inverted microscope.

Primary antibodies included goat anti-IBA1 (Abcam, Catlog#Ab5076, 1:500); rat anti-BrdU (Abcam, Catalog#:Ab6326, 1:200); rat anti-RFP(ChromoTek, Catalog#: 5f8-100, 1:1,000); rat anti CD68 (Bio-Rad; Catalog#: MCA1957); rabbit anti-IBA1(Wako, Catalog#:019-19741, 1:500); rabbit anti-FABP7 (Invitrogen, Catalog#:PA5-24949, 1:1,000); rabbit anti-STMN2(SCG10) (Novus a bio-techine, Catalog#:NBP1-49461, 1:1,000); rabbit anti ATF3 (Novus, Catalog#: NBP1-85816; 1:200); rabbit anti-dsRed (Takara, Catalog#:632496, 1:1,000) mouse anti TUJ1(β-tubulin) (Biolegend, Catalog#:801202, 1:1,000), mouse anti pERK (B-5) (Santa Cruz, Catalog# sc-377400,1:200), Chicken anti GFP(Abcam, Catalog#:ab13970, 1:1,000), Secondary antibodies conjugated to Alexa Fluor 488, Alexa Fluor 594 and Alexa Fluor 647 (Invitrogen) were diluted 1:500.

Single-Cell RNA Sequencing. L4 and L5 DRGs from 8-wk-old female mice were collected into cold dissection medium [HBSS (Thermofisher, Gibco; catlog#:14175-079)] with 10% 1M HEPES [(Thermofisher, Gibco; Catalog#15630080)], then transferred to fresh made prewarmed dissociation medium (15 U/mL Papain suspension (Worthington Biochemical; Catalog#LS003126), 0.3 mg/mL L-cysteine (Sigma; Catalog#C7352), 0.1 mg/mL Deoxyribonuclease I (Worthington Biochemical; Catalog#LS002139), 10% 1M HEPES in HBSS) incubated in 37 °C for 20 min. Samples were incubated with collagenase (150 μg/mL; Sigma; Catalog#C6885) in 37 °C for 20 min after washing with prewarmed HBSS twice. After washing with prewarmed HBSS twice, the single-cell suspension was resuspend by gently triturating in complete medium [Neurobasal™-A Medium, (Thermofisher, Gibco; Catalog# 12349015) with B-27™ Plus Supplement (Thermofisher, Gibco; Catalog# A3582801); GlutaMAX™ Supplement (Thermofisher, Gibco; Catalog#35050061)] followed by passing through 70-micron cell strainers. Single-cell suspension was resuspended in HBSS with 10% 1M HPEPS and 0.1% FBS (Thermofisher; Catalog# A3160401) followed by staining with LIVE/DEAD™ Fixable Aqua Dead Cell Stain Kit (ThermoFisher; Catalog# L34965). Live single cells were sorted by MoFlo (Beckman Coulter, Indianapolis, IN). Sorted cells were washed in PBS+0.04%BSA solution and manually counted using a hemocytometer. Solution was adjusted to a concentration of 700 to 1,000 cell/microliter and loaded on the 10X Chromium system. Single-cell RNA-Seq libraries were prepared using Chromium Next GEM Single Cell 3′ (v3.1 Kit) (10× Genomics). A digital expression matrix was obtained using 10X's CellRanger pipeline (Washington University The McDonnell Genome Institute). Quantification and statistical analysis were done with the Partek Flow package (Build version 10.0.21.0829).

Filtering criteria: Low–quality cells and potential doublets were filtered out from analysis using the following parameters: total reads per cell: 600 to 15,000, expressed genes per cell: 500 to 4,000, mitochondrial reads <10%. A noise reduction was applied to remove low expressing genes <=1 count. Counts were normalized and presented in logarithmic scale in count per million approach. An unbiased clustering (graph-based clustering) was done and presented as UMAP (Uniform Manifold Approximation and Projection), using a dimensional reduction algorithm that shows groups of similar cells as clusters on a scatter plot. Differential gene expression analysis performed using an ANOVA model; a gene is considered DE if it has an FDR < 0.05 and |fold-change| > 2. The data were subsequently analyzed for enrichment of KEGG pathways using Metascape (74).

Cell–Cell Interaction Analysis. The cell–cell interactions between different cell types in the DRG dataset were evaluated using CellChat (Version 1.4.0, R package). CellChat takes gene expression data as user input to model the probability of cell–cell communication by integrating gene expression with the existing database consisting of known interaction between signaling ligands, receptors, and their cofactors (55). In this paper, cell–cell interactions were analyzed individually for different conditions following the default pipeline. Normalized counts data from each condition were used to create CellChat object and applied the recommended preprocessing functions for the analysis of individual datasets with default parameters. CellChatDB.mouse was used as the database for inferring cell–cell communication. All categories of ligand–receptor interactions in the database were used in the analysis. Communications involving less than 10 cells were excluded.

Image Acquisition and Quantification. Confocal images were captured under the LSM880 confocal microscope (Carl Zeiss) unless otherwise specified. The images were captured under following parameters: 1 × optical zoom, scan speed 6, averaged 2 times, a pinhole of 1 AU, and 1,024 × 1,024 pixel size. The z-stack images were projected into overlay images using the "Maximum Intensity Projection" function in Zen Black software (Carl Zeiss). Sciatic nerve longitudinal images, the spinal cord, and brain images were captured under the EVOS™ M7000 Imaging System (Invitrogen). The images were captured under 10× objective in 1,980 × 1,080 pixel size. The stitched nerve images were generated by the EVOS imaging system. The neuronal culture images were captured under the ECLIPSE Ti2 inverted microscope (Nikon). The images were captured under 10× objective in 2,304 × 2,304 pixel size. Three tissue sections were analyzed on average for each independent mouse. For quantifying the number of $IBA1^+$, $tdTomato^+$, and $BrdU^+$ cells in the DRG, spinal cord and brain sections, the "cell counter" plug-in in Fiji was used. For quantifying macrophages in the sciatic nerve, the $IBA1^+$ and $tdTomato^+$ area was measured using "Analysis Particles" function in Fiji. Area, rather than the number, was measured in the nerve because the macrophages morphology appeared foam-like after injury. For quantifying the regeneration index in the injured sciatic nerve section, the highest SCG10 intensity along the nerve was defined as the crush site, as described (49), and confirmed by regional increased intensity of IBA1. The average SCG10 intensity at distances away from the crush site was normalized to the SCG10 intensity at the crush site using "measure" function in Fiji. For quantifying the neuron regenerative capacity in cultured DRG neurons, TUJ1-stained neurons were segmented by thresholding and subjected to neurite tracing using "Simple Neurite Tracer" plug-in in Fiji.

Statistical Analysis. All statistical analyses and graphs were conducted, organized, and generated in GraphPad Prism 9. Numerical data were presented as mean ± SD from at least two independent animals. The group mean difference was analyzed by either two-tailed unpaired Student's *t* test or one-way ANOVA with the Bonferroni post hoc test. For experiments including groups and multiple time-point measurements, data were analyzed by two-way ANOVA with the Bonferroni post hoc test. *P* values below 0.05 were considered as significant difference.

Data, Materials, and Software Availability. All software applications were commercially or freely available and are listed in the methods and resources table. All data reported are available and listed in *SI Appendix*, Reagent and resources table. The raw Fastq files and the processed filtered count matrix for single-cell RNA (scRNA) sequencing of DRGs from the PLX+CD diet group were deposited at the NCBI GEO database under the accession number GSE190283. The scRNA sequencing files of DRGs from the normal diet group were from GSE158892 (9).

ACKNOWLEDGMENTS. We would like to thank members of the Cavalli lab and Mokalled lab for valuable discussions and suggestions. We thank Dr. Qingyun Li and Dr. Jonathan Kipnis for constructive discussion and comments. We gratefully acknowledge Michael Savio from The Alvin J. Siteman Cancer Center at Barnes–Jewish Hospital and Washington University School of Medicine for assistance with single-cell sorting. We would like to thank Plexxikon Inc for

kindly providing the PLX73086 and PLX5622 compound and formulated diet. We show our gratitude and respect to all animals killed in this study. This work was funded in part by NIH grants R35 NS122260, R01 NS111719 and R21 NS115492 to V.C.

Author affiliations: [a]Department of Neuroscience, Washington University School of Medicine, St. Louis, MO 63110; [b]Department of Developmental Biology, Washington University School of Medicine, St. Louis, MO 63110; [c]Center of Regenerative Medicine, Washington University School of Medicine, St. Louis, MO 63110; and [d]Hope Center for Neurological Disorders, Washington University School of Medicine, St. Louis, MO 63110

1. D. S. Smith, J. H. Skene, A transcription-dependent switch controls competence of adult neurons for distinct modes of axon growth. *J. Neurosci.* **17**, 646–658 (1997).
2. Y. Cho *et al.*, Activating injury-responsive genes with hypoxia enhances axon regeneration through neuronal HIF-1alpha. *Neuron* **88**, 720–734 (2015).
3. I. Palmisano *et al.*, Epigenomic signatures underpin the axonal regenerative ability of dorsal root ganglia sensory neurons. *Nat. Neurosci.* **22**, 1913–1924 (2019).
4. F. J. Stam *et al.*, Identification of candidate transcriptional modulators involved in successful regeneration after nerve injury. *Euro. J. Neurosci.* **25**, 3629–3637 (2007).
5. M. Mahar, V. Cavalli, Intrinsic mechanisms of neuronal axon regeneration. *Nat. Rev. Neurosci.* **19**, 323–337 (2018).
6. E. E. Ewan *et al.*, Ascending dorsal column sensory neurons respond to spinal cord injury and downregulate genes related to lipid metabolism. *Sci. Rep.* **11**, 374 (2021).
7. W. Renthal *et al.*, Transcriptional reprogramming of distinct peripheral sensory neuron subtypes after axonal injury. *Neuron* **108**, 128–144.e9 (2020).
8. O. Avraham *et al.*, Satellite glial cells promote regenerative growth in sensory neurons. *Nat. Commun.* **11**, 4891 (2020).
9. O. Avraham *et al.*, Profiling sensory neuron microenvironment after peripheral and central axon injury reveals key pathways for neural repair. *Elife* **10**, e68457 (2021).
10. K. R. Jessen, R. Mirsky, The repair Schwann cell and its function in regenerating nerves. *J. Physiol.* **594**, 3521–3531 (2016).
11. M. Mueller *et al.*, Macrophage response to peripheral nerve injury: The quantitative contribution of resident and hematogenous macrophages. *Lab. Invest.* **83**, 175–185 (2003).
12. P. L. Wang *et al.*, Peripheral nerve resident macrophages share tissue-specific programming and features of activated microglia. *Nat. Commun.* **11**, 2552 (2020).
13. E. Ydens *et al.*, Profiling peripheral nerve macrophages reveals two macrophage subsets with distinct localization, transcriptome and response to injury. *Nat. Neurosci.* **23**, 676–689 (2020).
14. D. Pan *et al.*, The CCL2/CCR2 axis is critical to recruiting macrophages into acellular nerve allograft bridging a nerve gap to promote angiogenesis and regeneration. *Exp. Neurol.* **331**, 113363 (2020).
15. A. L. Cattin *et al.*, Macrophage-induced blood vessels guide schwann cell-mediated regeneration of peripheral nerves. *Cell* **162**, 1127–1139 (2015).
16. J. A. Stratton *et al.*, Macrophages regulate Schwann cell maturation after nerve injury. *Cell Rep.* **24**, 2561–2572.e6 (2018).
17. X. Lu, P. M. Richardson, Responses of macrophages in rat dorsal root ganglia following peripheral nerve injury. *J. Neurocytol.* **22**, 334–341 (1993).
18. M. J. Kwon *et al.*, Contribution of macrophages to enhanced regenerative capacity of dorsal root ganglia sensory neurons by conditioning injury. *J. Neurosci.* **33**, 15095–15108 (2013).
19. J. P. Niemi *et al.*, A critical role for macrophages near axotomized neuronal cell bodies in stimulating nerve regeneration. *J. Neurosci.* **33**, 16236–16248 (2013).
20. J. P. Niemi, A. DeFrancesco-Lisowitz, J. M. Cregg, M. Howarth, R. E. Zigmond, Overexpression of the monocyte chemokine CCL2 in dorsal root ganglion neurons causes a conditioning-like increase in neurite outgrowth and does so via a STAT3 dependent mechanism. *Exp. Neurol.* **275**, 25–37 (2016).
21. R. E. Zigmond, F. D. Echevarria, Macrophage biology in the peripheral nervous system after injury. *Prog. Neurobiol.* **173**, 102–121 (2019).
22. X. Yu *et al.*, Dorsal root ganglion macrophages contribute to both the initiation and persistence of neuropathic pain. *Nat. Commun.* **11**, 264 (2020).
23. J. Addington, M. Freimer, Chemotherapy-induced peripheral neuropathy: An update on the current understanding. *F1000Res* **5**, F1000 Faculty Rev-1466 (2016).
24. W. Kallenborn-Gerhardt *et al.*, Nox2-dependent signaling between macrophages and sensory neurons contributes to neuropathic pain hypersensitivity. *Pain* **155**, 2161–2170 (2014).
25. H. Zhang *et al.*, Dorsal root ganglion infiltration by macrophages contributes to paclitaxel chemotherapy-induced peripheral neuropathy. *J. Pain* **17**, 775–786 (2016).
26. A. L. Kalinski *et al.*, Analysis of the immune response to sciatic nerve injury identifies efferocytosis as a key mechanism of nerve debridement. *Elife* **9**, e60223 (2020).
27. R. Gentek, K. Molawi, M. H. Sieweke, Tissue macrophage identity and self-renewal. *Immunol. Rev.* **262**, 56–73 (2014).
28. V. Bellver-Landete *et al.*, Microglia are an essential component of the neuroprotective scar that forms after spinal cord injury. *Nat. Commun.* **10**, 518 (2019).
29. A. Krishnan, S. Bhavanam, D. Zochodne, An intimate role for adult dorsal root ganglia resident cycling cells in the generation of local macrophages and satellite glial cells. *J. Neuropathol. Exp. Neurol.* **77**, 929–941 (2018).
30. F. J. Pixley, E. R. Stanley, CSF-1 regulation of the wandering macrophage: Complexity in action. *Trends Cell Biol.* **14**, 628–638 (2004).
31. R. Seijffers, C. D. Mills, C. J. Woolf, ATF3 increases the intrinsic growth state of DRG neurons to enhance peripheral nerve regeneration. *J. Neurosci.* **27**, 7911–7920 (2007).
32. S. D. Holland, L. M. Ramer, S. B. McMahon, F. Denk, M. S. Ramer, An ATF3-CreERT2 Knock-in mouse for axotomy-induced genetic editing: Proof of principle. *eNeuro* **6**, ENEURO.0025-19.2019 (2019).
33. S. Yona *et al.*, Fate mapping reveals origins and dynamics of monocytes and tissue macrophages under homeostasis. *Immunity* **38**, 79–91 (2013).
34. Y. Huang *et al.*, Repopulated microglia are solely derived from the proliferation of residual microglia after acute depletion. *Nat. Neurosci.* **21**, 530–540 (2018).
35. S. E. Jager *et al.*, Changes in the transcriptional fingerprint of satellite glial cells following peripheral nerve injury. *Glia* **68**, 1375–1395 (2020).
36. A. A. Mapps *et al.*, Diversity of satellite glia in sympathetic and sensory ganglia. *Cell Rep.* **38**, 110328 (2022).
37. L. A. Green, J. C. Nebiolo, C. J. Smith, Microglia exit the CNS in spinal root avulsion. *PLoS Biol.* **17**, e3000159 (2019).
38. T. Kaiser, G. Feng, Tmem119-EGFP and Tmem119-CreERT2 transgenic mice for labeling and manipulating microglia. *eNeuro* **6**, ENEURO.0448-18.2019 (2019).
39. M. Prinz, D. Erny, N. Hagemeyer, Ontogeny and homeostasis of CNS myeloid cells. *Nat. Immunol.* **18**, 385–392 (2017).
40. F. Ginhoux *et al.*, Fate mapping analysis reveals that adult microglia derive from primitive macrophages. *Science* **330**, 841–845 (2010).
41. K. Kierdorf *et al.*, Microglia emerge from erythromyeloid precursors via Pu.1- and Irf8-dependent pathways. *Nat. Neurosci.* **16**, 273–280 (2013).
42. O. Matcovitch-Natan *et al.*, Microglia development follows a stepwise program to regulate brain homeostasis. *Science* **353**, aad8670 (2016).
43. H. Maruoka, K. Kubota, R. Kurokawa, S. Tsuruno, T. Hosoya, Periodic organization of a major subtype of pyramidal neurons in neocortical layer V. *J. Neurosci.* **31**, 18522–18542 (2011).
44. M. Donegan, M. Kernisant, C. Cua, L. Jasmin, P. T. Ohara, Satellite glial cell proliferation in the trigeminal ganglia after chronic constriction injury of the infraorbital nerve. *Glia* **61**, 2000–2008 (2013).
45. B. Huang *et al.*, Phenotypical peculiarities and species-specific differences of canine and murine satellite glial cells of spinal ganglia. *J. Cell Mol. Med.* **25**, 6909–6924 (2021).
46. L. Jasmin, J. P. Vit, A. Bhargava, P. T. Ohara, Can satellite glial cells be therapeutic targets for pain control? *Neuron Glia Biol.* **6**, 63–71 (2010).
47. A. A. Mapps *et al.*, Diversity of satellite glia in sympathetic and sensory ganglia. *Cell Rep* **38**, 110328 (2022).
48. M. van Velzen *et al.*, Neuron-interacting satellite glial cells in human trigeminal ganglia have an APC phenotype. *J. Immunol.* **183**, 2456–2461 (2009).
49. J. E. Shin, S. Geisler, A. DiAntonio, Dynamic regulation of SCG10 in regenerating axons after injury. *Exp. Neurol.* **252**, 1–11 (2014).
50. Y. Cho, R. Sloutsky, K. M. Naegle, V. Cavalli, Injury-induced HDAC5 nuclear export is essential for axon regeneration. *Cell* **155**, 894–908 (2013).
51. D. Carlin, A. E. Halevi, E. E. Ewan, A. M. Moore, V. Cavalli, Nociceptor deletion of Tsc2 enhances axon regeneration by inducing a conditioning injury response in dorsal root ganglia. *eNeuro* **6**, ENEURO.0168-19.2019 (2019).
52. O. Avraham *et al.*, Satellite glial cells promote regenerative growth in sensory neurons. *Nat. Commun.* **11**, 4891 (2020).
53. Y. L. Weng, J. Joseph, R. An, H. Song, G. L. Ming, Epigenetic regulation of axonal regenerative capacity. *Epigenomics* **8**, 1429–1442 (2016).
54. N. Sharma *et al.*, The emergence of transcriptional identity in somatosensory neurons. *Nature* **577**, 392–398 (2020).
55. S. Jin *et al.*, Inference and analysis of cell-cell communication using cell chat. *Nat. Commun.* **12**, 1088 (2021).
56. R. C. Meyer, M. M. Giddens, B. M. Coleman, R. A. Hall, The protective role of prosaposin and its receptors in the nervous system. *Brain Res.* **1585**, 1–12 (2014).
57. B. Liu *et al.*, Glio- and neuro-protection by prosaposin is mediated by orphan G-protein coupled receptors GPR37L1 and GPR37. *Glia* **66**, 2414–2426 (2018).
58. R. C. Meyer, M. M. Giddens, S. A. Schaefer, R. A. Hall, GPR37 and GPR37L1 are receptors for the neuroprotective and glioprotective factors prosaptide and prosaposin. *Proc. Natl. Acad. Sci. U.S.A.* **110**, 9529–9534 (2013).
59. C. G. Jolivalt, K. M. Ramos, K. Herbetsson, F. S. Esch, N. A. Calcutt, Therapeutic efficacy of prosaposin-derived peptide on different models of allodynia. *Pain* **121**, 14–21 (2006).
60. C. G. Jolivalt, Y. Vu, L. M. Mizisin, A. P. Mizisin, N. A. Calcutt, Impaired prosaposin secretion during nerve regeneration in diabetic rats and protection of nerve regeneration by a prosaposin-derived peptide. *J. Neuropathol. Exp. Neurol.* **67**, 702–710 (2008).
61. A. J. Shepherd *et al.*, Angiotensin II triggers peripheral macrophage-to-sensory neuron redox crosstalk to elicit pain. *J. Neurosci.* **38**, 7032–7057 (2018).
62. Y. Lavin *et al.*, Tissue-resident macrophage enhancer landscapes are shaped by the local microenvironment. *Cell* **159**, 1312–1326 (2014).
63. M. Guilliams, C. L. Scott, Does niche competition determine the origin of tissue-resident macrophages? *Nat. Rev. Immunol.* **17**, 451–460 (2017).
64. F. Zhang, E. Nance, Y. Alnasser, R. Kannan, S. Kannan, Microglial migration and interactions with dendrimer nanoparticles are altered in the presence of neuroinflammation. *J. Neuroinflammation* **13**, 65 (2016).
65. M. Tsuda, Microglia in the spinal cord and neuropathic pain. *J. Diabetes Investig.* **7**, 17–26 (2016).
66. N. Gu *et al.*, Spinal microgliosis due to resident microglial proliferation is required for pain hypersensitivity after peripheral nerve injury. *Cell Rep.* **16**, 605–614 (2016).
67. M. Hanani, D. C. Spray, Emerging importance of satellite glia in nervous system function and dysfunction. *Nat. Rev. Neurosci.* **21**, 485–498 (2020).
68. J. G. Mitterreiter *et al.*, Satellite glial cells in human trigeminal ganglia have a broad expression of functional Toll-like receptors. *Eur. J. Immunol.* **47**, 1181–1187 (2017).
69. M. Guilliams, F. R. Svedberg, Does tissue imprinting restrict macrophage plasticity? *Nat. Immunol.* **22**, 118–127 (2021).
70. A. Krishnan, S. Dwivedi, A. Chandrasekhar, A. Areti, D. W. Zochodne, In vitro priming response in dorsal root ganglia partially mimics injury-driven pre-conditioning response and reprograms neurons for enhanced outgrowth. *Mol. Cell Neurosci.* **110**, 103573 (2021).
71. B. T. Himes, A. Tessler, Death of some dorsal root ganglion neurons and plasticity of others following sciatic nerve section in adult and neonatal rats. *J. Comp. Neurol.* **284**, 215–230 (1989).
72. K. Obata *et al.*, Differential activation of MAPK in injured and uninjured DRG neurons following chronic constriction injury of the sciatic nerve in rats. *Eur. J. Neurosci.* **20**, 2881–2895 (2004).
73. L. Madisen *et al.*, A robust and high-throughput Cre reporting and characterization system for the whole mouse brain. *Nat. Neurosci.* **13**, 133–140 (2010).
74. Y. Zhou *et al.*, Metascape provides a biologist-oriented resource for the analysis of systems-level datasets. *Nat. Commun.* **10**, 1523 (2019).